

LST1 promotes the assembly of a molecular machinery responsible for tunneling nanotube formation

**Christian Schiller^{1,2}, Kalliope N. Diakopoulos¹, Ina Rohwedder¹, Elisabeth
Kremmer², Christine von Toerne³, Marius Ueffing³, Ulrich H. Weidle⁴, Hiroshi
Ohno⁵ and Elisabeth H. Weiss¹**

¹ Department of Biology II, Ludwigs-Maximilians-Universität München, Germany

² Institute of Molecular Immunology, Helmholtz Zentrum München, Germany

³ Research Unit Protein Science, Helmholtz Zentrum München, Germany

⁴ Roche Diagnostics, Division Pharma, Penzberg, Germany

⁵ Research Center for Allergy and Immunology, RIKEN, Yokohama, Japan

Correspondence to Prof. Dr. Elisabeth H. Weiss, Biozentrum der LMU, Grosshadernerstr. 2, 82152 Planegg-Martinsried, Germany. Phone: +49-89-218074317. Fax: +49-89-218074331. Email: elisabeth.weiss@lmu.de

Running head: LST1 induces the formation of nanotubes

Word count: 7500

Summary

Carefully orchestrated intercellular communication is an essential prerequisite for the development of multicellular organisms. In recent years, tunneling nanotubes (TNT) have emerged as a novel and widespread mechanism of cell-cell communication. However, the molecular basis of their formation is still poorly understood. In the present study we report that the transmembrane MHC class III protein LST1 induces the formation of functional nanotubes and is required for endogenous nanotube generation. Mechanistically, we found LST1 to induce nanotube formation by recruiting the small GTPase RalA to the plasma membrane and promoting its interaction with the exocyst complex. Furthermore, we determined LST1 to recruit the actin-crosslinking protein filamin to the plasma membrane and to interact with M-Sec, myosin and myoferlin. These results allow us to suggest a molecular model for nanotube generation. In this proposal LST1 functions as a membrane scaffold mediating the assembly of a multimolecular complex, which controls the formation of functional nanotubes.

Introduction

Recently, tunneling nanotubes (TNTs) have been established as a novel and widespread mechanism of intercellular communication, for a current review see (Abounit and Zurzolo, 2012). Nanotubes were originally characterized as long (up to several cell diameters) and thin (50 - 200 nm diameter) membrane extensions connecting rat PC12 cells (Rustom et al., 2004) and are thought to be the mammalian equivalent to cytonemes found in the *Drosophila* wing imaginal disc (Ramirez-Weber and Kornberg, 1999). Transfer of organelles (Rustom et al., 2004), soluble markers (Watkins and Salter 2005) and electrical signals (Wang et al., 2010) between distant cells connected via nanotubes has been observed and points to a pivotal role of these structures in cell-cell communication. Nanotubes have been found to connect a wide range of immune cells like B cells (Gupta and DeFranco, 2003), T cells (Sowinski et al., 2008), macrophages (Onfelt et al., 2004), mast cells (Fifadara et al., 2010), NK cells (Chauveau et al., 2010) and dendritic cells (Watkins and Salter, 2005). Interestingly, nanotubes have also been reported to connect dendritic cells in vivo in the mouse cornea (Chinnery et al., 2008). However, nanotubes are not present exclusively in immune cells but are rather widespread structures found in a growing number of cells from different tissues (Rustom et al., 2004; Wang et al., 2010; Wittig et al., 2012). The recent discovery that nanotubes may connect bacteria from different species (Dubey and Ben-Yehuda, 2011) indicates that nanotubes are not an exclusively eukaryotic trait but a common means of intercellular communication in nature. The *LST1* (*Leukocyte Specific Transcript 1*) gene is localized next to the TNF cluster of the HLA class III region (Holzinger et al., 1995) and is highly expressed in macrophages and dendritic cells (de Baey et al., 1997; Rollinger-Holzinger et al., 2000). While *LST1* transcript levels are highest in immune cells, we found the LST1 protein to be expressed at comparable levels in human cells of hematopoietic and non-hematopoietic origin (Schiller et al., 2009). LST1 expression is characterized by extensive alternative splicing. Depending on exon usage, the resulting isoforms are either short soluble molecules or transmembrane proteins. A definitive function for LST1 has not been determined yet, however, it has been proposed that LST1 isoforms play an important role in regulating the immune response (Rollinger-Holzinger et al., 2000) and enabling cell-cell communication (Raghunathan et al., 2001). Overexpression of transmembrane LST1 has been shown to induce the formation of thin membrane protrusions up to 300 μm in length, which display a striking resemblance to nanotubes (Raghunathan et al., 2001). The effect of LST1 overexpression on cell morphology led us to question whether LST1 transmembrane proteins are involved in the formation of tunneling nanotubes.

Results

LST1 overexpression induces the formation of tunneling nanotubes

The induction of long membrane protrusions caused by overexpression of LST1 transmembrane isoforms has been described previously (Raghunathan et al., 2001). We were able to confirm this finding by transiently overexpressing a transmembrane LST1-EGFP fusion protein in HeLa cells. Transfectants displayed numerous membrane protrusions (Fig. 1A), while cells expressing a transmembrane control fusion protein did not show an altered morphology (Fig. 1B). We found the LST1-induced membrane protrusions to be suspended above the substratum and to often connect distant cells (Fig. 1A, lower panel). This concordance with hallmark characteristics of tunneling nanotubes prompted us to term these structures TNT-like protrusions. Overexpression of LST1-EGFP led to a significant increase in the percentage of cells displaying TNT-like protrusions (Fig. 1C), similar results were obtained in other cell lines (supplementary material Fig. S1). The induction of TNT-like protrusions was not construct-specific, as the overexpression of a FLAG-LST1 protein yielded a similar effect (supplementary material Fig. S2A-C). A more detailed analysis of the LST1-induced TNT-like structures revealed that they were significantly longer than the ones observed between transfected control cells (Fig. 1D; supplementary material Fig. S2D-F). This result is in line with our observation that in LST1 transfectants, TNT-like structures with a span of up to 200 μm could be detected; while in transfected control cells the extent of these structures never surpassed 60 μm (data not shown). Furthermore, LST1-EGFP was enriched in TNT-like structures and in vesicles found therein (Fig. 1A, arrow; supplementary material Fig. S3A, arrow). Since nanotubes were initially described to contain actin but not tubulin (Rustom et al., 2004), we used this criterion to characterize the LST1-induced TNT-like structures. In transfectants overexpressing LST1-EGFP, we found TNT-like structures to be actin-rich but to contain only traces of tubulin (Fig. 1E). To enable a more sensitive detection of tubulin, transfectants coexpressing EGFP-tubulin and LST1-mCherry fusion proteins were imaged by live-cell confocal microscopy. Transfectants displayed TNT-like protrusions of different diameters and lengths; „thick“ and shorter protrusions clearly contained EGFP-tubulin while in „thin“ protrusions no EGFP-tubulin was detectable (Fig. 1F; supplementary material Fig. S3B, C). Our results suggest some heterogeneity in the LST1-induced TNT-like membrane protrusions, all structures contain actin but only structures of larger diameter enclose tubulin. These findings are in agreement with a report describing two classes of structurally distinct nanotubes (Onfelt et al., 2006). The functional significance of different types of cellular conduits is not known so far. A quantitative analysis of the two different types of TNT-like protrusions revealed LST1 to induce the formation of both classes

of structures (supplementary material Fig. S3G). In subsequent experiments we did not discriminate between thick and thin, long and short TNT-like protrusions. Further characterization revealed that the LST1-induced TNT-like protrusions were sensitive to fixation (supplementary material Fig. S3D) and therefore display the same sensitivity to mechanical stress as nanotubes (Rustom et al., 2004). This finding also allowed us to postulate that most of the „long“ membrane protrusions we observed in cells overexpressing LST1-EGFP (supplementary material Fig. S1) may actually be TNT-like structures brought in contact with the substratum by the mechanical stress of fixation. Cocultivation of cells overexpressing either LST1-EGFP or LST1-mCherry fusion proteins demonstrated that the TNT-like protrusions induced by LST1 are not remnant structures of cell division (supplementary material Fig. S3E). A potential role of LST1 in nanotube formation was further substantiated by our finding that endogenous LST1 is enriched in nanotubes connecting HeLa cells (supplementary material Fig. S3F). In summary, the detailed characterization of membrane protrusions observed in cells overexpressing LST1 allows us to conclude that these structures exhibit all the typical characteristics of tunneling nanotubes.

LST1 supports the formation of functional tunneling nanotubes

Nanotubes enable intercellular vesicle and/or organelle transport. To determine whether LST1-induced nanotubes were functional and could mediate cell-cell communication we discriminatively labelled LST1 and control transfected HeLa cells with the dyes CFSE (cytoplasm) and DiI (membrane/endocytic vesicles) followed by cocultivation (supplementary material Fig. S4). The percentage of CFSE-stained cells containing DiI-labelled vesicles was used as an indicator for the efficiency of nanotube-mediated transport. The vesicle transfer rate was significantly increased in cells overexpressing LST1 when compared to transfected control cells (Fig. 2A). This effect was not due to an increased rate of exosome secretion in cells overexpressing LST1 (supplementary material Fig. S5). Nanotube formation is dependent on actin polymerization (Gurke et al., 2008; Bukoreshtliev et al., 2009). Treatment of the cocultures with the inhibitor of actin polymerization latrunculin-A led to a decrease in vesicle transfer and completely abrogated the effect of LST1 overexpression on the transfer rate (Fig. 2A). Thus the observed effect depends on de novo actin polymerization. These results indicate that both LST1 and control transfected HeLa cells exchange vesicles and/or organelles via nanotubes and that LST1 overexpression induced the formation of additional functional nanotubes, which significantly enhanced the transfer rate in transfected cells. To determine whether LST1 is required for nanotube formation we stably transfected HeLa cells with a vector expressing shRNA targeting *LST1*. The downregulation of *LST1* protein expression was confirmed by western blot analysis (supplementary material Fig. S6). The effect of *LST1* knock down on the formation of functional nanotubes was examined as above. Knock down of *LST1*

resulted in a significant decrease of the vesicle transfer rate when compared to control transfectants (Fig. 2B). The negative effect of LST1 depletion on nanotube formation was confirmed by directly staining LST1 shRNA transfectants. *LST1* knock down resulted in a significant decrease in the percentage of cells displaying nanotubes (Fig. 2C). These results further support the notion that transmembrane LST1 is required for nanotube formation. To elucidate the molecular mechanism underlying LST1-induced nanotube formation we examined the role of small GTPases in this process. Small GTPases have been shown to be key regulators of cytoskeletal remodelling (Heasman et al., 2008). Moreover, the Ras-like small GTPase RalA has been shown to be required for nanotube formation (Hase et al., 2009). We coexpressed LST1-EGFP and mutant GTPases and evaluated their effects on nanotube formation. The expression of GTPases was monitored by western blot analysis (supplementary material Fig. S7). The mutants RalA-28N, Cdc42-17N and Rac1-17N exclusively bind GDP and therefore induce a dominant negative effect. Overexpression of RalA-28N completely blocked LST1-induced nanotube formation, while Cdc42-17N only caused a modest reduction and Rac1-17N had no effect (Fig. 2D). The mutants RalA-38R and RalA-48W do not interact with the exocyst components Sec5 and Exo84 respectively. Overexpression of both RalA-38R and RalA-48W also completely blocked LST1-induced nanotube formation (Fig. 2D). These results indicate that RalA and its interaction with components of the exocyst complex are required for LST1-induced nanotube formation. Our findings are in line with the results of Hase et al. who first reported a role for RalA and the exocyst complex in nanotube formation.

LST1 interacts with RalA, M-Sec and the exocyst complex

The finding that RalA and the exocyst complex are involved in LST1-induced nanotube formation prompted us to test whether these proteins interact directly. Coexpression of LST1-EGFP and Myc-RalA in HEK-293T cells, followed by immunoprecipitation revealed that Myc-RalA clearly coprecipitated with the LST1-EGFP fusion protein, but not with EGFP alone (Fig. 3A). The interaction between LST1 and RalA was confirmed in further experiments. Endogenous RalA coprecipitated with LST1-EGFP (Fig. 3B) and endogenous LST1 coprecipitated with a mCherry-RalA fusion protein (Fig. 3C). Having found several dominant negative RalA mutants to block LST1-induced nanotube formation, we tested whether these mutations impaired binding of RalA to LST1. However, we found all assayed mutant proteins to clearly coprecipitate with LST1-EGFP in comparable amounts (supplementary material Fig. S8A). This observation implies that LST1 interacts with RalA independently of whether GDP or GTP is bound. Next we examined a possible interaction between LST1 and the exocyst complex. We found Sec5 to clearly coprecipitate with LST1-EGFP but not with EGFP alone (Fig. 3D). Additional experiments revealed that further

Journal of Cell Science • Accepted manuscript

components of the exocyst complex also coprecipitated with LST1-EGFP, although to a lesser extent than Sec5 (supplementary material Fig. S8B, C). These results demonstrate that Sec5 is the main interacting protein for LST1 in the exocyst complex. RalA is a known interactor of Sec5 (Moskalenko et al., 2002); it is thus plausible that RalA mediates binding of LST1 to Sec5. To test this hypothesis, we coexpressed LST1-EGFP and either Myc-RalA, Myc-RalA-38R or a control vector. Overexpression of Myc-RalA did not enhance binding of LST1 to Sec5 (supplementary material Fig. S8D, E). On the other hand, overexpression of Myc-RalA-38R, a dominant negative mutant unable to bind to Sec5, did not impair the interaction between LST1 and Sec5 (supplementary material Fig. S8D, E). We therefore concluded that RalA does not mediate LST1-Sec5 binding and that these molecules interact directly. This finding prompted the question whether LST1 plays a role in the interaction between RalA and Sec5. To investigate this possibility we coexpressed mCherry-RalA and either LST1-EGFP or EGFP. Overexpression of LST1-EGFP significantly enhanced coprecipitation of Sec5 with mCherry-RalA (Fig. 3E, F). Thus we conclude that LST1 promotes the RalA-Sec5 interaction. Exo84, a further component of the exocyst complex has also been described to be an interactor of RalA (Moskalenko et al., 2003). However, overexpression of LST1-EGFP did not promote the RalA-Exo84 interaction (supplementary material Fig. S8F, G), indicating that LST1 selectively promotes the interaction between RalA and Sec5. In a previous study M-Sec was found to induce nanotube formation by interacting with RalA and signalling through the Ral-exocyst pathway (Hase et al., 2009). Further coprecipitation experiments revealed that LST1 clearly interacts with M-Sec (Fig. 3G). Taken together our results indicate that LST1 is a central component of the M-Sec-RalA-exocyst pathway, which controls nanotube formation.

LST1 recruits RalA to the plasma membrane

To gain further insights into the mechanism underlying LST1-induced nanotube formation, we characterized the interaction between RalA and LST1. In HeLa cells coexpressing LST1-EGFP and mCherry-RalA, both proteins colocalized in nanotubes (Fig. 4A; supplementary material Fig. S9A) and were enriched at the plasma membrane in sites of nanotube formation (Fig. 4B). Furthermore, we found overexpression of LST1-EGFP to significantly increase plasma membrane localization of mCherry-RalA (Fig. 4C–E). In control transfectants, mCherry-RalA localized to the plasma membrane and was also distributed throughout the cytoplasm and in internal membranes (Fig. 4C; supplementary material Fig. S9B), a subcellular allocation resembling that of endogenous RalA (Lim et al., 2010). In transfectants overexpressing LST1-EGFP, mCherry-RalA fusion protein at the plasma membrane predominated and was scarcely found in the cytoplasm and internal membranes (Fig. 4D; supplementary material Fig. S9C). This result indicates that RalA is recruited to the

plasma membrane by LST1 from a cytoplasmic RalA protein pool. Overexpression of mCherry-RalA in LST1 shRNA transfectants (see supplementary material Fig. S6) resulted in a modest but significant decrease in membrane localization (Fig. 4F). This result led us to conclude, that while LST1 promotes membrane localization of RalA it is probably not the only factor involved in this process. We confirmed our findings by performing fluorescence recovery after photobleaching (FRAP) experiments. The recovery of mCherry-RalA fluorescence at the plasma membrane was significantly accelerated by the presence of LST1-EGFP (Fig. 4G, H). Taken together, our results demonstrate that LST1 actively recruits RalA to the plasma membrane. Next, we examined the interaction between LST1 and Sec5 more closely. In cells overexpressing LST1-EGFP, endogenous Sec5 colocalized with the fusion protein at the cell membrane and in nanotubes (supplementary material Fig. S10A, B). In contrast to RalA, overexpression of LST1 did not lead to an increased membrane localization of Sec5 (supplementary material Fig. S10C, D). Therefore, we suggest that LST1 interacts with Sec5 and the exocyst complex directly at the plasma membrane but is not involved in membrane recruitment of exocyst components.

LST1 recruits filamin to the plasma membrane

Having shown that LST1 induces the formation of functional nanotubes by recruiting RalA to the plasma membrane and promoting its interaction with the exocyst complex, we searched for further LST1-interacting proteins, which may contribute to nanotube formation. Analysis of LST1-EGFP precipitates from a stable HeLa transfectant revealed a noticeable coprecipitated band above 175 kDa, which was absent in the precipitate from a control transfectant (Fig. 5A). Mass spectrometry analysis of this band identified filamin, myoferlin and the myosin II heavy chains MYH9/MYH10 (supplementary material Table S1). These proteins were also identified in a mass spectrometry analysis of LST1-EGFP precipitate from transiently transfected HEK-293T cells (supplementary material Table S2). The identified proteins were confirmed to interact with LST1 by western blot analysis (supplementary material Fig. S11). Filamin is an effector of RalA, and interacts with GTP-bound RalA (Ohta et al., 1999). Therefore we examined the role of filamin in LST1-induced nanotube formation. To test whether RalA mediates binding between LST1 and filamin, LST1-EGFP was coexpressed with either the control vector, Myc-RalA or Myc-RalA-28N, a constitutively GDP-bound dominant negative mutant unable to interact with filamin. Coexpression of recombinant Myc-RalA led to a significant increase in the amount of filamin coprecipitated with LST1-EGFP, while coexpression of the mutant Myc-RalA-28N resulted in a significant decrease of bound filamin (Fig. 5B, C). These results indicate that RalA mediates the interaction between LST1 and filamin. Staining of endogenous filamin in cells overexpressing LST1-EGFP revealed that both proteins colocalized at the cell membrane and in nanotubes (Fig. 5D). Furthermore, overexpression

of LST1-EGFP led to a significant increase in filamin membrane localization (Fig. 5D–F). However, coexpression of Myc-filamin with LST1-EGFP did not enhance the LST1-induced formation of nanotubes (supplementary material Fig. S12), indicating that filamin is not a limiting factor in this process. Taken together our results suggest that LST1 recruits filamin to the plasma membrane in a RalA-dependent manner.

Discussion

Recent research has established tunneling nanotubes as a novel means of intercellular communication between distant cells and these structures have also been shown to play a key role in a number of pathological processes. Several viruses have been revealed to specifically hijack nanotubes for intercellular transfer, invisible to the immune system, to promote their rapid spreading (Sherer et al., 2007; Sowinski et al., 2008; Eugenin et al., 2009; Mukerji et al., 2012). Furthermore, nanotubes allow the intercellular transfer of prion protein in vitro and may be involved in the spreading of infectious prions in vivo (Gousset et al., 2009). The relevance of nanotube-mediated cell-cell communication in these pathological processes emphasizes the importance to understand the mechanisms by which cells regulate nanotube formation. In the present study we show that the transmembrane MHC class III protein LST1 induces the formation of functional tunneling nanotubes (Fig. 1). Furthermore, LST1 knock down reduces endogenous nanotube formation and impairs intercellular vesicle transfer (Fig. 2). Therefore, we postulate a molecular mechanism for the involvement of LST1 in nanotube formation. However, since LST1 knock down did not completely abrogate TNT formation and vesicle transfer, either residual LST1 protein is sufficient to partially enable the formation of nanotubes, and/or alternative LST1-independent mechanisms exist. Tunneling nanotubes have been detected in immune cells, but also in cells from a wide range of tissues. *LST1* mRNA expression is predominant in immune cells (de Baey et al., 1997; Rollinger-Holzinger et al., 2000). However, in a previous study we found the full-length, transmembrane LST1 protein to be present in human cells of haematopoietic and non-haematopoietic origin at comparable levels (Schiller et al., 2009). The widespread expression implies that its involvement in nanotube formation may not be restricted to immune cells. Furthermore, transmembrane LST1 is highly conserved in mammals (data not shown), pointing to an evolutionarily conserved function in nanotube genesis. Recently, Hase et al. reported a role for RalA and the exocyst complex in nanotube formation. In their study, M-Sec was described to promote nanotube formation by binding to RalA, which in turn interacted with the exocyst complex. However, it remained unclear, how the cytoplasmic protein M-Sec would be able to orchestrate the processes required to induce nanotubes. Coprecipitation and mass spectrometry analysis revealed interactions between LST1, RalA, M-Sec, filamin and several components of the exocyst complex (Fig. 3, 5; supplementary material Fig. S8, 11). The small GTPase RalA is a central regulator of cytoskeletal remodelling and exerts this function by signalling through three pathways: RalA targets filamin, an actin-crosslinking protein (Ohta et al., 1999), RalA mediates the assembly of the exocyst complex, which in turn regulates actin polymerization by activating the Arp2/3 complex (Jin et al., 2005; Zuo et al., 2006) and finally, RalA induces cytoskeletal remodelling by binding RalBP1, which activates Cdc42 (Ikeda et al., 1998). The recruitment of

RalA to the plasma membrane by LST1 and the RalA-dependent interaction between LST1 and filamin indicates that LST1 may direct actin-crosslinking to specific sites of the plasma membrane (Fig. 4). Our finding, that overexpression of filamin does not further enhance LST1-induced formation of nanotubes indicates that endogenous filamin protein levels are not a limiting factor in this process. The enhancement of the RalA-Sec5 interaction by LST1 (Fig. 3) raises the possibility that LST1 induces actin polymerization by promoting the RalA-mediated assembly of the exocyst complex. However, the role of the exocyst complex in the formation of nanotubes may not be restricted to the regulation of actin polymerization but could also involve membrane complementation by tethering vesicles to discrete regions of the plasma membrane. Hase et al. reported that the RalA-RalBP1-Cdc42 pathway may play a role in the elongation of nanotubes but is not central to their formation. Since a dominant negative mutant of Cdc42 only slightly inhibited LST1-induced nanotube formation (Fig. 2), we conclude that the LST1-RalA-filamin and LST1-RalA-exocyst pathways constitute the central mechanisms of this process, while Cdc42 probably only plays a minor role. Further coprecipitation and mass spectrometry analyses revealed that LST1 interacts with myoferlin and the myosin II heavy chains MYH9/MYH10 (Fig. 5). Myosin Ib and myosin IIa have been shown to promote the formation and scission of tubules at the trans-Golgi network by locally deforming the membrane and increasing membrane tension, respectively (Almeida et al., 2011; Miserey-Lenkei et al., 2010). The formation of long membrane protrusions like nanotubes would also require directed plasma membrane deformation, a process that could be mediated by myosin. Myoferlin is a member of the ferlin family and has been shown to enable membrane fusion between myoblasts (Doherty et al., 2005). Nanotubes establish cytoplasmic continuity between distant cells. This process requires punctual membrane fusion, which could be facilitated by myoferlin. However, it also appears feasible that the transmembrane LST1 protein itself is involved in membrane fusion. Nanotube-inducing LST1 isoforms are small asymmetric transmembrane polypeptides lacking a cleavable signal sequence that use an internal reverse signal-anchor sequence for membrane insertion. They feature a glycine/leucine-rich transmembrane region followed by basic amino acid residues, structural motifs also found in fusion-associated small transmembrane (FAST) proteins encoded by fusogenic reoviruses (Clancy and Duncan, 2009). In summary, the results of this study allow us to propose a molecular model for the formation of LST1-induced tunneling nanotubes (Fig. 6). In this model, LST1 acts as a membrane scaffold for the assembly of a multiprotein complex that orchestrates the formation of nanotubes. Two pathways for membrane and cytoskeletal reorganization converge on LST1 at the plasma membrane, thereby spatially linking key processes, which are essential for the formation of LST1-induced nanotubes. First, LST1 recruits the small GTPase RalA and its effector filamin to the plasma membrane, thereby inducing localized actin-crosslinking. Second, LST1 promotes the interaction between RalA and the exocyst complex at the plasma membrane, thereby enabling exocyst-mediated actin

polymerization and membrane complementation. Additionally, the known inducer of nanotube formation M-Sec interacts with LST1 and RalA. The identification of myosin and myoferlin as LST1-interacting proteins raises the possibility that these proteins may contribute to the formation of open-ended nanotubes by locally deforming the plasma membrane and enabling membrane fusion. The mechanisms that trigger TNT protuberance remain unknown. Based on our model for LST1-induced TNT formation it seems plausible that enrichment of LST1 at specific sites of the plasma membrane may be the initial step. This event may be regulated by modification of LST1, since tyrosine phosphorylation and palmitoylation have been described (Draber et al., 2012). Plasma membrane accumulation of LST1 could also depend on cofactors not identified in this study.

Materials and methods

Generation of expression constructs

The EGFP-tubulin fusion vector was obtained from Clontech. The Myc-RalA-28N, Myc-RalA-38R, Myc-RalA-48W, Myc-Cdc42-17N and Myc-Rac1-17N expression constructs have been described previously (Hase et al., 2009). The Myc-filamin-A expression construct was a gift from John Blenis (Woo et al., 2004 ; Addgene plasmid #8982). A construct for the expression of wild-type Myc-RalA was generated using the Myc-RalA-28N expression construct and the Phusion site-directed mutagenesis kit from Finnzymes, following the manufacturer's instructions. Tagged expression constructs were created by fusing the sequence encoding the FLAG epitope with the appropriate cDNA using a semi-nested PCR approach. *LST1* transcripts were amplified as described (Schiller et al., 2009). The FLAG-LST1.2345 insertion (encoding the full-length transmembrane isoform, named by exon usage) was cloned into the pcDNA 3.1 (-) expression vector (Invitrogen). The FLAG-LST1.2345 insertion was also cloned in frame into the pEGFP-N1 vector (Clontech). Additionally, the FLAG-LST1.2345 ORF was fused to cDNA encoding the red fluorescent protein mCherry (Shaner et al., 2004) and inserted into the pcDNA 3.1 (+) vector (Invitrogen), thus creating the LST1-mCherry fusion construct. A mCherry-RalA fusion construct was generated in the same manner by amplification of the wild-type RalA ORF. For the KIR2DS2-EGFP transmembrane control fusion construct, cDNA was amplified using primers specific for KIR2DS2 and cloned into the pEGFP-N1 vector. For the FLAG-DAP12 transmembrane control construct, cDNA was amplified using primers specific for DAP12 and cloned into the pcDNA 3.1 (+) vector. The shRNA vectors for *LST1* knock down were purchased from SABiosciences and contained the following insertions: LST1: 5'-CAAGCTCTGGATGAGGAACTT-3' and Control: 5'-GGAATCTCATTCGATGCATAC-3'.

Antibodies and reagents

Monoclonal antibodies against the FLAG (M2) and Myc (9E10) epitopes were obtained from Sigma-Aldrich and Roche, respectively. The monoclonal antibody against filamin (FLMN01) was from Dianova. The monoclonal antibody against RFP (5F8) used to detect mCherry has been described previously (Rottach et al., 2008). The monoclonal antibody against tubulin (WA-3) was a kind gift from M. Schliwa (Ludwig-Maximilians-Universität München, Germany). The generation of a monoclonal antibody against LST1 for use in western blot procedures (7E2) was described in a previous report (Schiller et al., 2009), an additional antibody for use in immunocytochemistry (2B1) was generated for the present study. Polyclonal antibodies against Exo70 (H-300), Exo84 (C-16), Sec6 (H-230), MYH9 (H-40), MYH10 (H-46) and myoferlin (H-111) were obtained from Santa

Cruz Biotechnology. Polyclonal antibodies against GFP, RalA and Sec5 were from Invitrogen, Millipore and Proteintech, respectively. TRITC-labelled phalloidin was from Sigma-Aldrich. For immunocytochemistry the following secondary antibodies were used: Alexa488-conjugated chicken anti-rat (Invitrogen), Cy5-conjugated goat anti-mouse and DyLight649-conjugated goat anti-rabbit (both from Jackson). For western blot analysis IRDye800CW-conjugated goat anti-mouse, anti-rat and anti-rabbit antibodies were used (Li-Cor).

Cell culture, transfection and immunocytochemistry procedures

HeLa (ATCC CCL-2.1), U2-OS (ATCC HTB-96) and HEK-293T (ATCC CRL-11268) cells were cultivated as recommended by ATCC. HeLa and U2-OS cells were transfected with Lipofectamine 2000 (Invitrogen), following the manufacturer's instructions and using a 1:1 DNA/reagent ratio. HEK-293T cells were transfected using PEI (Sigma-Aldrich) with the DNA/reagent ratio 1:4. Transfectants were analyzed 24 hours after transfection. HeLa stable transfectants were established by cultivation in growth medium containing 2 mg/ml G418 (PAA). Resulting clones were screened by FACS and western analysis. For immunocytochemistry cells were seeded on polylysine-coated cover slips, washed with PBS containing 0.02% Tween-20, fixated in 2% PFA + 0.1% GTA for 5 min and permeabilized with PBS + 0.1% Triton X-100. Blocking was performed with PBS + 3% BSA. To prevent disruption of nanotubes all steps were performed avoiding direct light and wash steps were conducted without removing the entire liquid.

Cocultivation and vesicle transfer assay

HeLa cells were transfected as described above, transfection efficiency was monitored via FACS analysis and staining was performed as previously described (Schiller et al., 2009). Cocultivation experiments were only performed if transfection efficiency was at least 65% (usual range 68 – 79%). Transfectants were stained either with CFSE or DiI (both from Invitrogen) according to the manufacturer's instructions and cocultivated on polylysine coated cover slips for 6 hours prior to fixation. Treatment with latrunculin-A (Sigma-Aldrich) was performed at a concentration of 500 nM for 5 hours. The cells were allowed to adhere for 1 hour before treatment with latrunculin-A, because direct treatment prevents adhesion. Thus, a certain background is observed due to vesicle transfer in this first hour of coculture, as described previously (Rustom et al., 2004). For each cover slip at least 100 random CFSE-stained cells were imaged by fluorescence microscopy. Images were scored for CFSE-stained cells containing DiI-stained vesicles and/or organelles by two independent observers (C.S. and I.R.). Organelle transfer rates were obtained by averaging the scores determined by the two observers.

Immunoprecipitation, isolation of exosomes and western blot analysis

The immunoprecipitation of GFP or mCherry was performed using the GFP-Trap A or RFP-Trap A reagents from Chromotek. Exosomes were isolated by differential centrifugation (100000 g pellet) following an established protocol (Théry et al., 2006). Western blot analysis was performed as described before (Schiller et al., 2009); blot imaging and signal quantification were conducted using the Odyssey infrared imaging system (Li-Cor). For quantitative analysis, western blots were imaged at least three times using different excitation intensities.

Microscopy

For microscopy of fixated cells, cover slips were embedded in Vectashield (Vector Laboratories), for live-cell microscopy cells were seeded out in 35 mm μ -dishes (Ibidi) and Opti-MEM medium (Gibco). Fluorescence microscopy was performed on a TE 2000 S eclipse microscope (Nikon) using a 60x/1.25 NA plan oil immersion objective and a C-8484 camera (Hamamatsu Photonics). Images were acquired with the Wasabi software (version 2.0, Hamamatsu Photonics). Confocal microscopy was performed on a TCS-SP5 confocal laser scanning microscope (Leica) equipped with a 63x/1.4 NA plan-apochromat oil immersion objective. Fluorophores were excited with 488, 561 and 633 nm laser lines. Images were acquired with the LAS AF software (version 2.0, Leica). For live-cell confocal microscopy the TCS-SP5 microscope was equipped with a heated chamber set to 37°C. For FRAP analysis of EGFP and mCherry-fused proteins, confocal image series were acquired with a frame size of 256 \times 256 pixels and a pixel size of 100 nm. Plasma membrane sections measuring 7 \times 1,5 μ m were photobleached for 300 ms with the 458, 476, 488, 496, 514, 561 and 596 nm laser lines set to maximum power at 100% transmission. Typically 20 pre-bleach (150 ms time interval) and 120 post-bleach (500 ms time interval) frames were recorded for each series. Quantitative evaluation was performed using the ImageJ software (version 1.44, NIH). The mean fluorescence intensities from all frames were background subtracted and normalized to the mean of the last 10 pre-bleach values. For each series the time for recovery of 50% of pre-bleach fluorescence intensity was calculated.

Mass spectrometry procedures

The gel pieces were reduced with 5 mM DTT for 15 min at 60°C and acetylated using freshly prepared 25 mM iodacetamide (IAA) solution for 15 min at room temperature in the dark. Then 0.01 μ g/ μ l trypsin solution (Sigma) in 50 mM ABC (ammonium bicarbonate) was added and after incubation for 10 min, 25 mM ABC was added to cover the gel pieces completely during digest at 37°C over night. For elution, 100 μ l of 60% ACN (acetonitril) / 0.1% TFA (trifluoroacetic acid) were added to the gel cubes and incubated for 15 minutes with shaking. The supernatant was transferred to a new tube and 100 μ l of 99.9% ACN/0.1% TFA were added to the gel pieces. After

additional 30 min of incubation, the supernatants were pooled. The supernatants containing the eluted peptides were dried in a speedvac (UniEquip) and stored at -20°C. Dried prefractionation samples were thawed and dissolved in 60 μ l of 2% ACN/0.5% TFA for 30 min at RT under agitation. Before loading, the samples were centrifuged for 5 min at 4°C. LC-MS/MS analysis was performed as described previously (Hauck et al., 2010), with a 120 min LC-gradient from 5 to 31% of buffer B (80% acetonitrile, 0.1% formic acid in HPLC-grade water) at 300 nl/min flow rate followed by a short 5-min gradient from 31 to 95% buffer B. From the MS prescan, the 10 most abundant peptide ions were selected for fragmentation with at least 200 counts and at least doubly charged. During fragment analysis a high-resolution (60,000 full-width half maximum) MS spectrum was acquired in the Orbitrap with a mass range from 200 to 1500 Da. The lock mass option was activated and every ion selected for fragmentation was excluded for 30 s by dynamic exclusion. The acquired spectra were loaded to the Progenesis software (version 2.5, Nonlinear) for label free quantification and analyzed as described previously (Hauck et al., 2010).

Statistical analysis

Differences between groups were tested for significance by applying the Mann-Whitney-U-test, using the BrightStat software (Stricker, 2008). Differences were considered significant at $p < 0.05$.

Acknowledgements

We would like to thank Stefanie Färberböck and Verena Kircher for excellent technical assistance. We would also like to thank Andrea Rottach for providing the RFP antibody and assisting with confocal microscopy. Latrunculin-A was a kind gift from Michael Schleicher. The KIR2DS2-EGFP and FLAG-DAP12 expression vectors were cloned by Eva Schlecker. The LST1-mCherry fusion construct was cloned by Gerlinde Puster. Bettina Nowak, Claudia Martin, Marisa Kurz, Laura Posselt and Anna Ullraum contributed to this report as part of the undergraduate research program. This work was supported by the Helmholtz Zentrum München PhD Program, Research Field „Infection and Immunity“.

Author contributions

C.S. designed and performed experiments, and wrote the paper. K.N.D. and I.R. performed experiments and helped with data analysis. E.K. generated antibodies. C.v.T. and M.U. performed mass spectrometry experiments. H.O. provided expression constructs and wrote the paper. E.H.W. supervised the project and wrote the paper with U.H.W. and C.S.

References

- Abounit, S. and Zurzolo, C.** (2012). Wiring through tunneling nanotubes--from electrical signals to organelle transfer. *J. Cell Sci.* **125**, 1089-98.
- Almeida, C. G., Yamada, A., Tenza, D., Louvard, D., Raposo, G. and Coudrier, E.** (2011). Myosin 1b promotes the formation of post-Golgi carriers by regulating actin assembly and membrane remodelling at the trans-Golgi network. *Nat. Cell Biol.* **13**, 779-89.
- Bukoreshtliev, N. V., Wang, X., Hodneland, E., Gurke, S., Barroso, J. F. and Gerdes, H. H.** (2009). Selective block of tunneling nanotube (TNT) formation inhibits intercellular organelle transfer between PC12 cells. *FEBS Lett.* **583**, 1481-8.
- Chauveau, A., Aucher, A., Eissmann, P., Vivier, E. and Davis, D. M.** (2010). Membrane nanotubes facilitate long-distance interactions between natural killer cells and target cells. *Proc. Natl. Acad. Sci. USA.* **107**, 5545-50.
- Chinnery, H. R., Pearlman, E. and McMenamin, P. G.** (2008). Cutting edge: Membrane nanotubes in vivo: a feature of MHC class II+ cells in the mouse cornea. *J. Immunol.* **180**, 5779-83.
- Clancy, E. K. and Duncan, R.** (2009). Reovirus FAST protein transmembrane domains function in a modular, primary sequence-independent manner to mediate cell-cell membrane fusion. *J. Virol.* **83**, 2941-50.
- Davis, D. M. and Sowinski, S.** (2008). Membrane nanotubes: dynamic long-distance connections between animal cells. *Nat. Rev. Mol. Cell Biol.* **9**, 431-6.
- de Baey, A., Fellerhoff, B., Maier, S., Martinozzi, S., Weidle, U. and Weiss, E. H.** (1997). Complex expression pattern of the TNF region gene LST1 through differential regulation, initiation, and alternative splicing. *Genomics.* **45**, 591-600.
- Doherty, K. R., Cave, A., Davis, D. B., Delmonte, A. J., Posey, A., Earley, J. U., Hadhazy, M. and McNally, E. M.** (2005). Normal myoblast fusion requires myoferlin. *Development.* **132**, 5565-75.

Draber, P., Stepanek, O., Hrdinka, M., Drobek, A., Chmatal, L., Mala, L., Ormsby, T., Angelisova, P., Horejsi, V. and Brdicka, T. (2012). LST1/A is a myeloid leukocyte-specific transmembrane adaptor protein recruiting protein tyrosine phosphatases SHP-1 and SHP-2 to the plasma membrane. *J. Biol. Chem.* **287**, 22812-21.

Dubey, G. P. and Ben-Yehuda, S. (2011). Intercellular nanotubes mediate bacterial communication. *Cell.* **144**, 590-600.

Eugenin, E. A., Gaskill, P. J. and Berman, J. W. (2009). Tunneling nanotubes (TNT) are induced by HIV-infection of macrophages: a potential mechanism for intercellular HIV trafficking. *Cell. Immunol.* **254**, 142-8.

Fifadara, N. H., Beer, F., Ono, S. and Ono, S. J. (2010). Interaction between activated chemokine receptor 1 and FcepsilonRI at membrane rafts promotes communication and F-actin-rich cytoneme extensions between mast cells. *Int. Immunol.* **22**, 113-28.

Gousset, K., Schiff, E., Langevin, C., Marijanovic, Z., Caputo, A., Browman, D. T., Chenouard, N., de Chaumont, F., Martino, A., Enninga, J., Olivo-Marin, J. C., Männel, D. and Zurzolo, C. (2009). Prions hijack tunnelling nanotubes for intercellular spread. *Nat. Cell Biol.* **11**, 328-36.

Gupta, N. and DeFranco, A. L. (2003). Visualizing lipid raft dynamics and early signaling events during antigen receptor-mediated B-lymphocyte activation. *Mol. Biol. Cell.* **14**, 432-44.

Gurke, S., Barroso, J. F., Hodneland, E., Bukoreshtliev, N. V., Schlicker, O. and Gerdes, H. H. (2008). Tunneling nanotube (TNT)-like structures facilitate a constitutive, actomyosin-dependent exchange of endocytic organelles between normal rat kidney cells. *Exp. Cell Res.* **314**, 3669-83.

Hase, K., Kimura, S., Takatsu, H., Ohmae, M., Kawano, S., Kitamura, H., Ito, M., Watarai, H., Hazelett, C. C., Yeaman, C. and Ohno, H. (2009). M-Sec promotes membrane nanotube formation by interacting with Ral and the exocyst complex. *Nat. Cell Biol.* **11**, 1427-32.

Hauck, S. M., Dietter, J., Kramer, R. L., Hofmaier, F., Zipplies, J. K., Amann, B., Feuchtinger, A., Deeg, C. A. and Ueffing, M. (2010). Deciphering membrane-associated

molecular processes in target tissue of autoimmune uveitis by label-free quantitative mass spectrometry. *Mol. Cell. Proteomics*. **9**, 2292-305.

Heasman, S. J. and Ridley, A. J. (2008). Mammalian Rho GTPases: new insights into their functions from in vivo studies. *Nat. Rev. Mol. Cell Biol.* **9**, 690-701.

Holzinger, I., de Baey, A., Messer, G., Kick, G., Zwierzina, H. and Weiss, E. H. (1995). Cloning and genomic characterization of LST1: a new gene in the human TNF region. *Immunogenetics*. **42**, 315-22.

Ikeda, M., Ishida, O., Hinoi, T., Kishida, S. and Kikuchi, A. (1998). Identification and characterization of a novel protein interacting with Ral-binding protein 1, a putative effector protein of Ral. *J. Biol. Chem.* **273**, 814-21.

Jin, R., Junutula, J. R., Matern, H. T., Ervin, K. E., Scheller, R. H. and Brunger, A. T. (2005). Exo84 and Sec5 are competitive regulatory Sec6/8 effectors to the RalA GTPase. *EMBO J.* **24**, 2064-74.

Lim, K. H., Brady, D. C., Kashatus, D. F., Ancrile, B. B., Der, C. J., Cox, A. D. and Counter, C. M. (2010). Aurora-A phosphorylates, activates, and relocalizes the small GTPase RalA. *Mol. Cell. Biol.* **30**, 508-23.

Mattila, P. K. and Lappalainen, P. (2008). Filopodia: molecular architecture and cellular functions. *Nat. Rev. Mol. Cell Biol.* **9**, 446-54.

Miserey-Lenkei, S., Chalancon, G., Bardin, S., Formstecher, E., Goud, B. and Echard, A. (2010). Rab and actomyosin-dependent fission of transport vesicles at the Golgi complex. *Nat. Cell Biol.* **12**, 645-54.

Moskalenko, S., Henry, D. O., Rosse, C., Mirey, G., Camonis, J. H. and White, M. A. (2002). The exocyst is a Ral effector complex. *Nat. Cell Biol.* **4**, 66-72.

Moskalenko, S., Tong, C., Rosse, C., Mirey, G., Formstecher, E., Daviet, L., Camonis, J. and White, M. A. (2003). Ral GTPases regulate exocyst assembly through dual subunit interactions. *J. Biol. Chem.* **278**, 51743-8.

Mukerji, J., Olivieri, K. C., Misra, V., Agopian, K. A. and Gabuzda, D. (2012). Proteomic analysis of HIV-1 Nef cellular binding partners reveals a role for exocyst complex proteins in mediating enhancement of intercellular nanotube formation. *Retrovirology*. **9**, 33.

Ohta, Y., Suzuki, N., Nakamura, S., Hartwig, J. H. and Stossel, T. P. (1999). The small GTPase RalA targets filamin to induce filopodia. *Proc. Natl. Acad. Sci. USA*. **96**, 2122-8.

Onfelt, B., Nedvetzki, S., Yanagi, K. and Davis, D. M. (2004). Cutting edge: Membrane nanotubes connect immune cells. *J. Immunol.* **173**, 1511-3.

Onfelt, B., Nedvetzki, S., Benninger, R. K., Purbhoo, M. A., Sowinski, S., Hume, A. N., Seabra, M. C., Neil, M. A., French, P. M. and Davis, D. M. (2006). Structurally distinct membrane nanotubes between human macrophages support long-distance vesicular traffic or surfing of bacteria. *J. Immunol.* **177**, 8476-83.

Raghunathan, A., Sivakamasundari, R., Wolenski, J., Poddar, R., and Weissman, S. M. (2001). Functional analysis of B144/LST1: a gene in the tumor necrosis factor cluster that induces formation of long filopodia in eukaryotic cells. *Exp. Cell Res.* **262**, 230-44.

Ramírez-Weber, F. A. and Kornberg, T. B. (1999). Cytonemes: cellular processes that project to the principal signaling center in *Drosophila* imaginal discs. *Cell*. **97**, 599-607.

Rollinger-Holzinger, I., Eibl, B., Pauly, M., Griesser, U., Hentges, F., Auer, B., Pall, G., Schratzberger, P., Niederwieser, D., Weiss, E. H. and Zwierzina, H. (2000). LST1: a gene with extensive alternative splicing and immunomodulatory function. *J. Immunol.* **164**, 3169-76.

Rottach, A., Kremmer, E., Nowak, D., Leonhardt, H. and Cardoso, M. C. (2008). Generation and characterization of a rat monoclonal antibody specific for multiple red fluorescent proteins. *Hybridoma*. **27**, 337-43.

Rustom, A., Saffrich, R., Markovic, I., Walther, P. and Gerdes, H. H. (2004). Nanotubular highways for intercellular organelle transport. *Science*. **303**, 1007-10.

Schiller, C., Nitschké, M. J., Seidl, A., Kremmer, E. and Weiss, E. H. (2009). Rat monoclonal antibodies specific for LST1 proteins. *Hybridoma*. **28**, 281-6.

Shaner, N. C., Campbell, R. E., Steinbach, P. A., Giepmans, B. N., Palmer, A. E. and Tsien, R. Y. (2004). Improved monomeric red, orange and yellow fluorescent proteins derived from *Discosoma* sp. red fluorescent protein. *Nat. Biotechnol.* **22**, 1567-72.

Sherer, N. M., Lehmann, M. J., Jimenez-Soto, L. F., Horensavitz, C., Pypaert, M. and Mothes, W. (2007). Retroviruses can establish filopodial bridges for efficient cell-to-cell transmission. *Nat. Cell Biol.* **9**, 310-5.

Sowinski, S., Jolly, C., Berninghausen, O., Purbhoo, M. A., Chauveau, A., Köhler, K., Oddos, S., Eissmann, P., Brodsky, F. M., Hopkins, C., Onfelt, B., Sattentau, Q. and Davis, D. M. (2008). Membrane nanotubes physically connect T cells over long distances presenting a novel route for HIV-1 transmission. *Nat. Cell Biol.* **10**, 211-9.

Stricker, D. (2008). BrightStat.com: free statistics online. *Comput. Methods Programs Biomed.* **92**, 135-43.

Théry, C., Amigorena, S., Raposo, G. and Clayton, A. (2006). Isolation and characterization of exosomes from cell culture supernatants and biological fluids. *Curr. Protoc. Cell Biol.* Chapter 3: Unit 3.22.

Wang, X., Veruki, M. L., Bukoreshtliev, N. V., Hartveit, E. and Gerdes, H. H. (2010). Animal cells connected by nanotubes can be electrically coupled through interposed gap-junction channels. *Proc. Natl. Acad. Sci. USA.* **107**, 17194-99.

Watkins, S. C. and Salter, R. D. (2005). Functional connectivity between immune cells mediated by tunneling nanotubules. *Immunity.* **23**, 309-18.

Wittig, D., Wang, X., Walter, C., Gerdes, H. H., Funk, R. H. and Roehlecke, C. (2012). Multi-level communication of human retinal pigment epithelial cells via tunneling nanotubes. *PLoS One.* **7**, e33195.

Woo, M. S., Ohta, Y., Rabinovitz, I., Stossel, T. P. and Blenis, J. (2004). Ribosomal S6 kinase (RSK) regulates phosphorylation of filamin A on an important regulatory site. *Mol. Cell. Biol.* **24**, 3025-35.

Zuo, X., Zhang, J., Zhang, Y., Hsu, S. C., Zhou, D. and Guo, W. (2006). Exo70 interacts with the Arp2/3 complex and regulates cell migration. *Nat. Cell Biol.* **8**, 1383-8.

Figure Legends

Figure 1. LST1 induces the formation of tunneling nanotubes. (A, B, E and F) Maximum intensity projections of confocal z-slides, images at the substratum plane were not included. Scale bar: 20 μm . (A and B) HeLa cells were transfected with constructs encoding either transmembrane LST1-EGFP (A) or a transmembrane KIR2DS2-EGFP control fusion protein (B). Overexpression of LST1-EGFP induced the formation of TNT-like protrusions (A) while KIR2DS2-EGFP readily localized to the plasma membrane but did not cause morphological changes in transfected cells (B). TNT-like structures lacked contact with the substratum and were often found to connect LST1-EGFP transfectants (A, lower panel, yz-projection including the substratum plane). Note that the TNT-like structure contains an LST1-EGFP-enriched vesicle (A, arrow). (C and D) HeLa cells overexpressing LST1-EGFP or the control fusion protein were imaged by confocal microscopy, scored for the presence of TNT-like structures (C) and the length of these structures was measured (D). Protrusions connecting cells that lacked contact with the substratum were termed TNT-like protrusions. Mean values are indicated within the columns \pm s.d. The formation of TNT-like structures was significantly increased ($p = 0.009$) in LST1-EGFP transfectants when compared with cells expressing the control fusion protein (C). TNT-like structures formed by LST1-transfectants were also significantly longer ($p = 0.009$) than the ones observed between control transfectants (D). At least 200 cells were analyzed per group in 5 independent experiments. (E) HeLa cells overexpressing LST1-EGFP were stained for actin and tubulin. TNT-like protrusions connecting transfectants contained LST1-EGFP and actin (E, left and middle insets) but only trace amounts of tubulin (E, right inset, not visible). Note that the membrane protrusion was damaged by the mechanical stress of fixation and subsequent immunocytochemistry (E, arrow). (F) HeLa cells coexpressing LST1-mCherry (red) and EGFP-tubulin (green) were imaged by live-cell confocal microscopy. Transfectants were connected by LST1-induced membrane protrusions that lacked contact with the substratum (F, lower panel, yz-projection including the substratum plane, corresponding to the upper arrow). Thick membrane protrusions (F, asterisk) contained LST1 and tubulin while in thin membrane protrusions only LST1 could be detected (F, arrows).

Figure 2. LST1 supports the formation of functional nanotubes. Mean values are indicated within the columns \pm s.d. (A) HeLa cells transfected with a construct encoding FLAG-LST1 or a control vector (pcDNA 3.1) were stained with CFSE or DiI and cocultivated. The number of CFSE-positive cells containing DiI-stained vesicles and/or organelles was assessed by fluorescence microscopy as a measure of nanotube-mediated intercellular transfer. Transfer of stained organelles was significantly increased ($p = 0.009$) between cells overexpressing LST1 in comparison to control

transfectants. At least 500 cells were analyzed per group in 5 independent experiments. HeLa cells were transfected and stained as above, additionally cocultures were treated with the inhibitor of actin polymerization latrunculin-A. Treated cells displayed comparable vesicle transfer rates that were substantially reduced when compared with untreated cells. At least 300 cells were analyzed per group in 3 independent experiments. **(B)** Stable HeLa transfectants expressing shRNA targeting *LST1* or a control shRNA were analyzed as in (A). Transfer of stained organelles was significantly decreased ($p = 0.049$) in *LST1* shRNA transfectants when compared to control transfectants. At least 300 cells were analyzed per group in 3 independent experiments. **(C)** Stable HeLa transfectants expressing shRNA targeting *LST1* or a control shRNA were stained with the membrane dye DiI, imaged via confocal microscopy and scored for the presence of nanotubes. *LST1* shRNA transfectants displayed significantly decreased ($p = 0.009$) nanotube formation when compared to cells expressing the control shRNA. At least 200 cells were analyzed per group in 5 independent experiments. **(D)** HeLa cells were cotransfected with the *LST1*-EGFP construct and constructs for the expression of the mutants RalA-28N, RalA-38R, RalA-48W, Cdc42-17N, Rac1-17N or a control vector (pcDNA 3), imaged by confocal microscopy and scored for the presence of nanotubes. Overexpression of RalA-28N, RalA-38R and RalA-48W led to a significant reduction ($p = 0.009$) in nanotube formation when compared to control transfected cells and completely blocked the effect of *LST1*-EGFP overexpression. The overexpression of Cdc42-17N slightly inhibited nanotube formation while Rac1-17N had no effect. At least 200 cells were analyzed per group in 5 independent experiments.

Figure 3. *LST1* interacts with RalA, M-Sec and the exocyst complex. The indicated proteins were overexpressed in HEK-293T cells, followed by lysis and GFP or RFP-specific immunoprecipitation. Precipitates were probed via western blot analysis using the indicated antibodies. The positions of detected proteins and relevant molecular weight marker bands are indicated. **(A)** Recombinant Myc-RalA clearly coprecipitated with the *LST1*-EGFP fusion protein, but not with EGFP alone (A, upper panel). To ensure that comparable amounts of Myc-RalA were expressed, lysates were probed for the recombinant protein (A, middle panel). **(B-D)** In similar experiments, endogenous RalA was found to coprecipitate with *LST1*-EGFP (B) and endogenous *LST1* coprecipitated with a mCherry-RalA fusion protein (C). Additionally, endogenous Sec5, a component of the exocyst complex, was found to clearly coprecipitate with *LST1*-EGFP (D). **(E-F)** To investigate whether *LST1* influences the interaction between RalA and Sec5, mCherry-RalA was coexpressed either with *LST1*-EGFP or EGFP. Coexpression of *LST1*-EGFP visibly enhanced coprecipitation of Sec5 with mCherry-RalA (E). Quantitative western blot analysis of coprecipitation between Sec5 and mCherry-RalA (F). The Sec5 signal intensity was quantified and

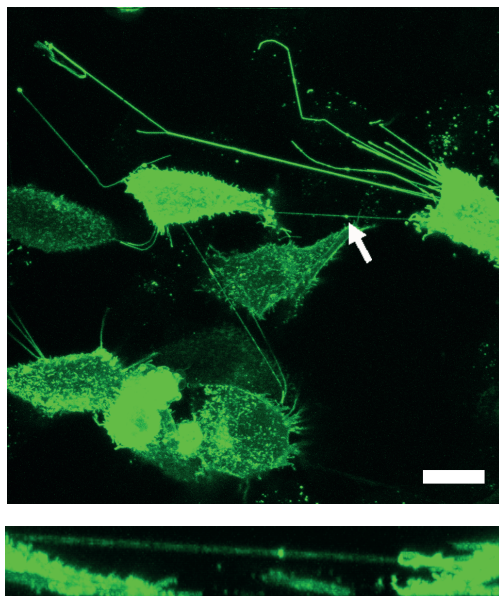
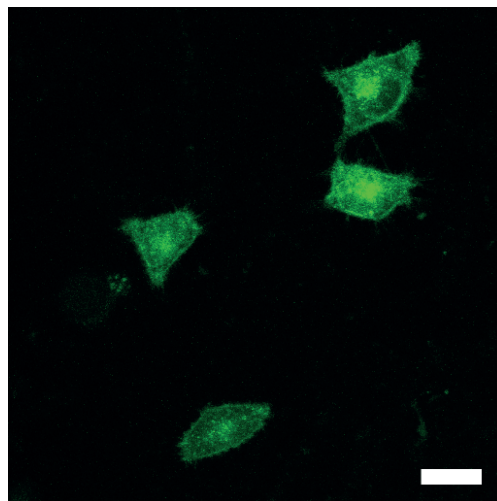
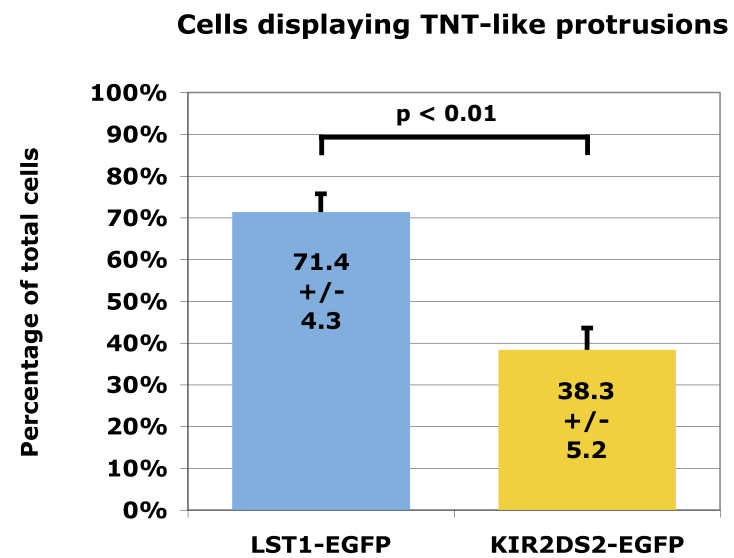
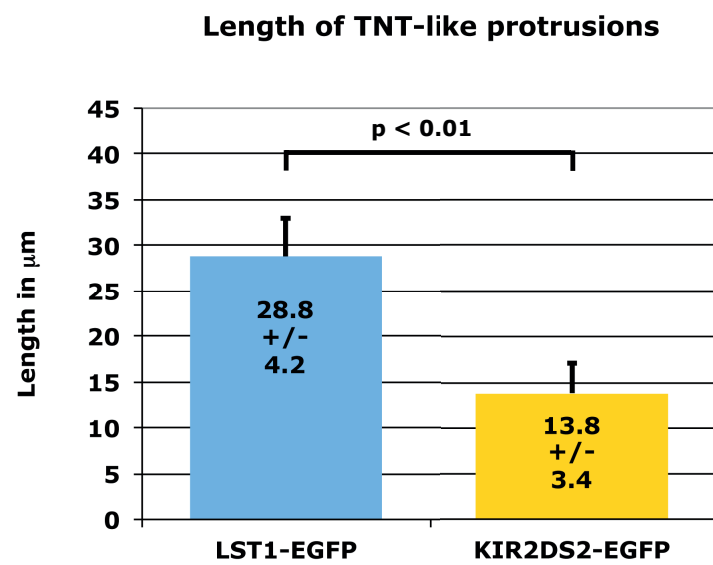
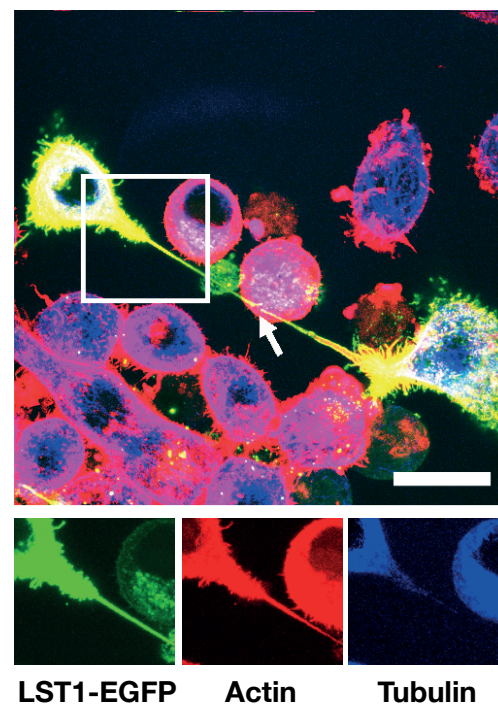
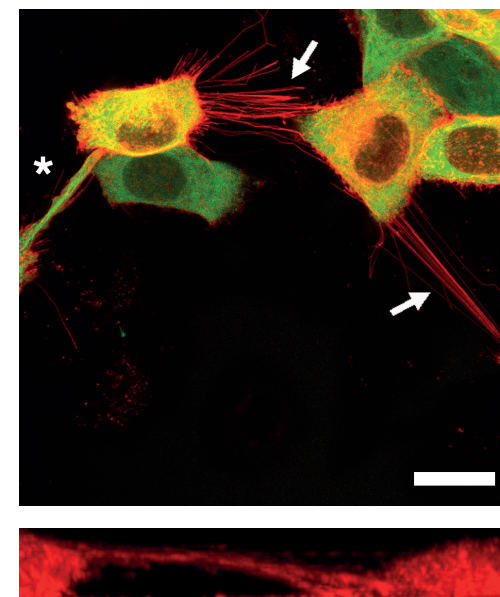
normalized for the amount of mCherry-RalA precipitated. Mean values from 5 independent experiments are indicated within the columns \pm s.d. Overexpression of LST1-EGFP significantly ($p = 0.009$) increased coprecipitation of Sec5 with mCherry-RalA. **(G)** M-Sec is a known inducer of nanotube formation (Hase et al., 2009). The LST1-mCherry fusion protein, but not mCherry alone coprecipitated with M-Sec-EGFP.

Figure 4. LST1 recruits RalA to the plasma membrane. (A-D) Maximum intensity projections of confocal z-slides (A, B) and single z-slides (C, D), images at the substratum plane were not included. Scale bar: 20 μ m. LST1-EGFP (green) and mCherry-RalA (red) were coexpressed in HeLa cells, both fusion proteins colocalized at the cell membrane and were present in nanotubes (A, zoom ups). Both fusion proteins were clearly enriched at the base of nanotubes, when compared to other positions of the plasma membrane (B, zoom ups). HeLa cells were cotransfected with constructs encoding mCherry-RalA and either EGFP (C) or LST1-EGFP (D). In cells overexpressing EGFP, mCherry-RalA was localized at the plasma membrane, but also throughout the cytoplasm and in internal membranes (C), while in transfectants overexpressing LST1-EGFP, the mCherry-RalA fusion protein localized primarily to the plasma membrane and was scarcely found throughout the cytoplasm (D). **(E-F)** Quantitative analysis of RalA membrane localization. The fluorescence intensity of mCherry-RalA at the plasma membrane was measured and compared to the total fluorescence intensity in 8 z-slides per cell. Mean values are indicated within the columns \pm s.d. At least 30 cells were analyzed per group in 3 independent experiments. In cells overexpressing LST1-EGFP, the mCherry-RalA fusion protein displayed a significantly ($p = 1.01E-11$) increased localization to the cell membrane, when compared with transfectants expressing EGFP only. In cells expressing a shRNA targeting *LST1*, mCherry-RalA membrane localization was significantly decreased ($p = 0.0002$) when compared to transfectants expressing an unspecific shRNA. **(G)** Fluorescence recovery after photobleaching (FRAP) analysis of mCherry-RalA. Cells were cotransfected as described above, mCherry-RalA was bleached at the plasma membrane and fluorescence recovery was tracked. The time point $t = 0$ was defined as immediately following bleaching, the fluorescence intensity is displayed as percentage of pre-bleaching fluorescence. A representative pair of data sets is displayed. mCherry-RalA membrane fluorescence clearly recovers more swiftly in cells coexpressing LST1-EGFP, when compared with transfectants coexpressing EGFP alone. **(H)** Quantitative analysis of mCherry-RalA fluorescence recovery. FRAP was performed as described above and the time required for the recovery of 50% pre-bleach fluorescence intensity was measured. Mean values are indicated within the columns \pm s.d. Fluorescence recovery of mCherry-RalA was significantly accelerated ($p = 9.78E-8$) in cells

coexpressing LST1-EGFP, when compared with transfectants coexpressing EGFP alone. At least 30 cells were analyzed per group in 3 independent experiments.

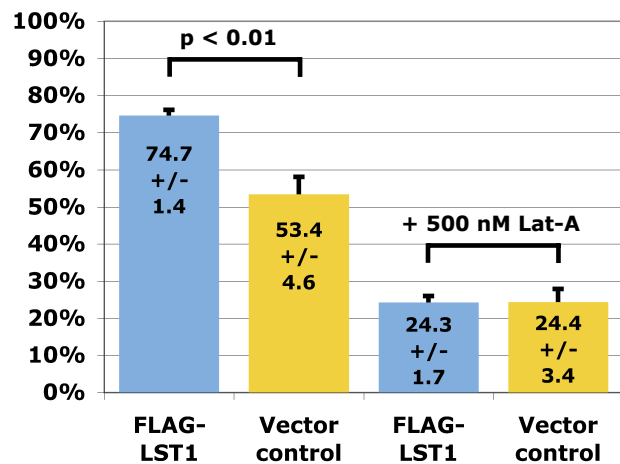
Figure 5. LST1 recruits filamin to the plasma membrane. (A) Stable HeLa transfectants expressing either LST1-EGFP or EGFP were lysed followed by GFP-specific immunoprecipitation. Precipitates were separated via PAGE and proteins were visualized using coomassie staining. The positions of detected proteins and relevant molecular weight marker bands are indicated. A noticeable band above 175 kDa coprecipitated with LST1-EGFP but not with EGFP (bounding boxes). Mass spectrometry analysis of the coprecipitated band identified filamin, myoferlin and the myosin II heavy chains MYH9/MYH10. (B) To examine whether the interaction between LST1 and filamin is mediated by RalA, LST1-EGFP was coexpressed in HEK-293T cells either with a control vector (pcDNA 3), Myc-RalA or Myc-RalA-28N, a dominant negative mutant that is constitutively GDP-bound and is therefore unable to bind filamin. The LST1-EGFP fusion protein was immunoprecipitated and precipitates were separated both on 6% (upper panel) and 15% (lower panels) PAGE gels and examined via western blot analysis using the indicated antibodies. Additionally, coprecipitated RalA was detected to ensure that its interaction with LST1-EGFP was comparable in all samples (lower panel). (C) Quantitative western blot analysis of coprecipitation between filamin and LST1-EGFP. The filamin signal intensity was quantified and normalized for the amount of LST1-EGFP precipitated. Mean values from 4 independent experiments are indicated within the columns +/- s.d. Overexpression of Myc-RalA significantly ($p = 0.028$) increased coprecipitation of filamin with LST1-EGFP, while overexpression of Myc-RalA-28N significantly ($p = 0.028$) reduced the amount of filamin that coprecipitated with LST1-EGFP. (D-E) Maximum intensity projections of confocal z-slides, images at the substratum plane were not included. Scale bar: 20 μm . LST1-EGFP (green) was expressed in HeLa cells, which were stained for endogenous filamin (red), both proteins colocalized at the cell membrane and in nanotubes (d, zoom up). In cells overexpressing LST1-EGFP, endogenous filamin was enriched at the plasma membrane (D), while in transfectants overexpressing EGFP, enrichment of endogenous filamin at the plasma membrane was not detected (E). (F) Quantitative analysis of filamin membrane localization. Cells were transfected as described above, the fluorescence intensity of filamin at the plasma membrane was measured and compared to the total fluorescence intensity in 8 z-slides per cell. Mean values are indicated within the columns +/- s.d. In cells overexpressing LST1-EGFP, endogenous filamin displayed a significantly ($p = 4.23\text{E-}11$) increased localization to the cell membrane, when compared with transfectants expressing EGFP only. At least 30 cells were analyzed per group in 3 independent experiments.

Figure 6. Proposed model for the LST1-induced formation of tunneling nanotubes. Arrows indicate interactions, “R” indicates plasma membrane recruitment by LST1 and “+” denotes promotion of interaction by LST1. Transmembrane LST1 acts as a membrane scaffold for the assembly of a multiprotein complex that orchestrates the formation of nanotubes. In our proposed model two pathways for membrane and cytoskeletal reorganization converge on LST1 at the plasma membrane. First, LST1 recruits the small GTPase RalA and its effector filamin to the plasma membrane, thereby inducing localized actin-crosslinking. Second, LST1 promotes the interaction between RalA and the exocyst complex at the plasma membrane, thereby enabling exocyst-mediated actin polymerization and membrane complementation. Additionally, the known inducer of nanotube formation M-Sec interacts with LST1 and RalA. The identification of myosin and myoferlin as further LST1-interacting proteins indicates that these proteins may contribute to the formation of open-ended nanotubes by locally deforming the plasma membrane and enabling membrane fusion.

A**B****C****D****E****F**

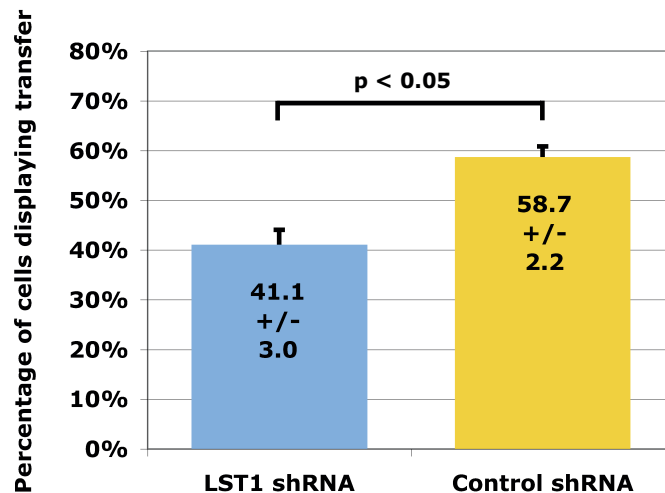
A

Transfer of DiI-stained vesicles



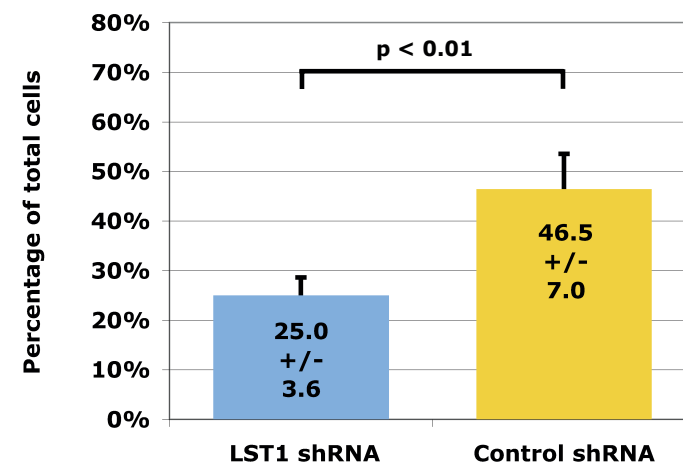
B

Transfer of DiI-stained vesicles



C

Cells displaying TNTs



D

Cells displaying TNTs

